Nanomedicine: Nanotechnology, Biology, and Medicine
14 (2018) 801–810

nanomedicine
Nanotechnology, Biology, and Medicine

nanomedjournal.com

Absolute sizing and label-free identification of extracellular vesicles by flow cytometry

Edwin van der Pol[a,b,c,*], Leonie de Rond, MSc[a,b,c], Frank A.W. Coumans[a,b,c], Elmar L. Gool, MSc[a,b,c], Anita N. Böing[b,c], Auguste Sturk[b,c], Rienk Nieuwland[b,c], Ton G. van Leeuwen[a,c]

[a]*Biomedical Engineering & Physics, University of Amsterdam, Amsterdam, The Netherlands*
[b]*Laboratory Experimental Clinical Chemistry, University of Amsterdam, Amsterdam, The Netherlands*
[c]*Vesicle Observation Center, Academic Medical Center, University of Amsterdam, Amsterdam, The Netherlands*

Received 10 August 2017; accepted 15 December 2017

Abstract

Blood contains extracellular vesicles (EVs), which are biological nanoparticles with clinical applications. In blood plasma, EVs are outnumbered by similar-sized lipoprotein particles (LPs), leading to controversial data such as non-specific binding of antibodies to LPs. Flow cytometry is a clinically applicable technique to characterize single EVs in body fluids. However, flow cytometry data have arbitrary units, impeding standardization, data comparison, and data interpretation, such as differentiation between EVs and LPs. Here we present a new method, named flow cytometry scatter ratio (Flow-SR), to relate the ambiguous light scattering signals of flow cytometry to the diameter and refractive index (RI) of single nanoparticles between 200-500 nm in diameter. Flow-SR enables label-free differentiation between EVs and LPs and improves data interpretation and comparison. Because Flow-SR is easy to implement, widely applicable, and more accurate and faster than existing techniques to size nanoparticles in suspension, Flow-SR has numerous applications in nanomedicine.

Key words: Drug delivery; extracellular vesicles; exosomes; flow cytometry; nanomedicine; nanoparticles

Extracellular vesicles (EVs), such as exosomes and microvesicles, are biological nanoparticles that are released by cells into the blood to transport waste and exchange intercellular messages, such as DNA, RNA, and surface receptors.[1] Because the size, concentration, composition and function of EVs change with disease, EVs are excellent candidates for early biomarkers of common diseases including cancer[2–4] and thrombosis.[5] Moreover, modified EVs are currently being examined as therapeutic agents.[6–8] Consequently, the scientific interest in EVs is thriving.

Figure 1*A* shows a typical transmission electron microscopy (TEM) image of EVs and lipoprotein particles (LPs) from the cell-depleted supernatant of a blood bank platelet concentrate. The figure reveals two key problems which the research field is facing: (1) most EVs have a diameter <500 nm and are therefore difficult to detect and study,[9] and (2) EVs are outnumbered by other similar-sized nanoparticles.[10–12] Especially blood plasma contains an abundance of nanoparticle types, such as LPs and high molecular weight proteins, which overlap in size with EVs.[10–12] Despite the development of novel methods to isolate EVs,[11,13] co-isolation of contaminants and loss of EVs remains unavoidable. For example, this co-isolation has led to confusion regarding the contributions of EVs and LPs as carriers of microRNA (miRNA) in human plasma.[12,14–16] To minimize the

Funding: Part of this work is supported by the Cancer-ID program (www.utwente.nl/tnw/cancer-id) and the MEMPHISII program of the Netherlands Technology Foundation STW, and the European Metrology Research Programme (EMRP) under the Joint Research Project HLT02 (www.metves.eu). The EMRP is jointly funded by the EMRP participating countries within the European Association of National Metrology Institutes and the European Union.

Acknowledgements: The authors would like to acknowledge A.E. Grootemaat for excellent experimental support.

*Corresponding author.
E-mail address: e.vanderpol@amc.uva.nl (E. van der Pol).

https://doi.org/10.1016/j.nano.2017.12.012

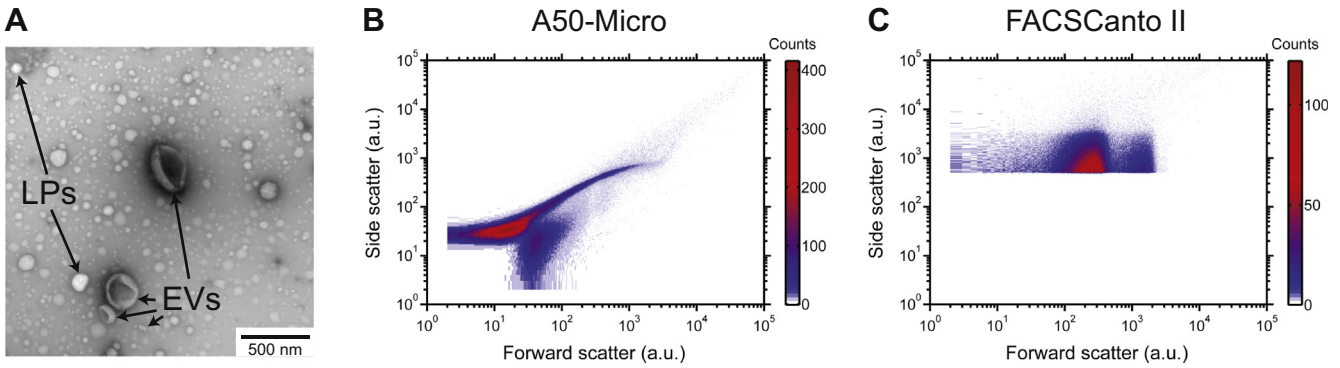

Figure 1. Flow cytometry data are typically presented in arbitrary units (a.u.), which hampers data interpretation and impedes data comparison. (**A**) Transmission electron microscopy (TEM) image of extracellular vesicles (EVs) and lipoprotein particles (LPs) from the cell-depleted supernatant of a platelet concentrate. The sample is polydisperse and all particles have a diameter <500 nm. EVs have a cup-shaped or homogeneous morphology and a diameter ≥30 nm. LPs are typically lighter than EVs, have a homogeneous morphology, but can also be smaller than 30 nm. (**B** and **C**) Scatter plots of side versus forward scatter of nanoparticles from the cell-depleted supernatant of a platelet concentrate measured by two different flow cytometers. The flow cytometry data cannot be mutually compared or related to the TEM data.

effect of an isolation method on measurement outcome, flow cytometry can be used to identify and characterize EVs directly in (diluted) plasma.[17] Due to the high throughput and multiplex fluorescence capabilities, flow cytometry is currently a promising and therefore a widely used technique to study single EVs in a clinical setting.[18]

To characterize EVs, state-of-the-art flow cytometers detect the forward scattered light (FSC), side scattered light (SSC), and fluorescence of single EVs beyond kHz rate.[19] Figure 1, *B* and *C* show the SSC-FSC scatter plots of EVs and LPs from the cell-depleted supernatant of a platelet concentrate measured by two different flow cytometers (A50-Micro, Apogee Flow Systems, UK; FACSCanto II, Becton Dickinson, USA). Because light scattering is a complex process, which depends on the size and refractive index (RI) of nanoparticles and the optical configuration of the flow cytometer, FSC and SSC are presented in arbitrary units. The arbitrary units, however, cause problems with data interpretation, data comparison and standardization. For example, from the scatter plots it is unclear which events correspond to the EVs of interest and what the diameter of the EVs is. Consequently, the scatter plots cannot be related to data generated by other analytical methods, such as TEM (Figure 1*A*). Moreover, different flow cytometers provide different scatter plots for the same sample, thereby impeding data comparison and multicenter research. These shortcomings of data representation lead to a 10^3-fold difference in the reported concentration of platelet EVs in blood plasma of healthy individuals[20] and caused scientists to study empty cells instead of the envisioned EVs.[21,22] In sum, more accurate, reproducible, and accessible methods to characterize EVs are urgently needed.

Here we introduce a new method to derive the diameter and RI of single nanoparticles from the FSC and SSC intensities of a flow cytometer. Direct access to the EV diameter in SI units solves the flow cytometry related problems with data interpretation, data comparison and standardization. Moreover, we demonstrate label-free differentiation between EVs and LPs based on differences in their RI, thereby solving a key problem of the research field.

Methods

Sample preparation

Beads (Supplementary Table 1) used to calibrate the FSC and SSC signals (Figure 2) were diluted in 50 nm filtered (Nuclepore, GE Healthcare, USA) purified and deionized water to a concentration of 10^6 mL^{-1}. The bead mixture (Supplementary Table 2) used to validate size and refractive index determination (Figure 3) was diluted to a total concentration of $3{\cdot}10^7$ mL^{-1} ($5{\cdot}10^6$ mL^{-1} for each population). Reference values of the bead diameters were obtained from the manufacturer specifications for the Thermo Fisher Scientific beads, an inter-laboratory comparison study for the Microparticles GmbH beads,[23] and TEM for the Kisker Biotech GmbH beads. Oil emulsions were diluted 4-fold (RI=1.36) and 10^6-fold (RI=1.40) and gold nanoparticles were diluted 100-fold in 50 nm filtered purified and deionized water. Intralipid was diluted 10^7-fold in 50 nm filtered phosphate-buffered saline (PBS; 1.54 mol L^{-1} NaCl, 12.4 mmol L^{-1} Na_2HPO_4, 2.05 mmol L^{-1} NaH_2PO_4, pH 7.4).

EVs and LPs (Figure 4, *A-C*) were isolated from an outdated platelet concentrate (Platelets, Sanquin, The Netherlands). The platelet concentrate (30 mL) was diluted 1:1 with 0.22 μm filtered (Millipore, Merck chemicals, Germany) PBS. Next, 12 mL acid citrate dextrose (0.85 mol L^{-1} trisodiumcitrate, 0.11 mol L^{-1} D-glucose and 0.071 mol L^{-1} citric acid) was added and the suspension was centrifuged (20 minutes, 800·*g*, 20 °C). The supernatant was isolated and 3-fold centrifuged (20 minutes, 1,550·*g*, 20 °C) to ensure complete removal of platelets. Cell-depleted plasma aliquots of 1 mL were frozen in liquid nitrogen and stored at -80 °C. Prior to the measurement, cell-depleted plasma was thawed on ice and incubated for 15 minutes with 1.5 μg mL^{-1} phycoerythrin (PE)-conjugated CD61 (555754, Becton Dickinson, USA) and, as a control, with

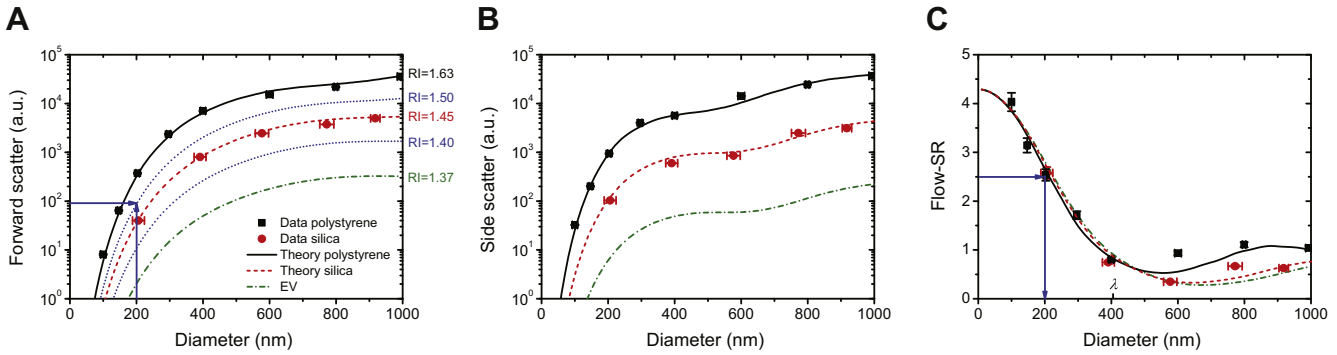

Figure 2. Size and refractive index (RI) determination of nanoparticles by the flow cytometry scatter ratio (Flow-SR). (**A**) Forward scatter, (**B**) side scatter, and (**C**) Flow-SR (side scatter/forward scatter) versus diameter as measured (symbols) and calculated (lines) for polystyrene (squares, solid line), silica (circles, dashed line) beads, extracellular vesicles (EV; dash dotted line), and particles with a refractive index of 1.40 and 1.50 (dotted lines). Forward scatter or side scatter cannot be individually related to diameter without knowledge of the RI of a particle. However, Flow-SR as a function of diameter is independent of the RI for nanoparticles with a diameter ≤1.2 times the illumination wavelength (λ). The arrows in panel (**C**) show how the diameter of a 200 nm nanoparticle can be obtained by Flow-SR. The arrows in panel (**A**) show how the RI of a 200 nm polystyrene bead can be obtained from the measured forward scatter once the diameter is known from Flow-SR.

1.5 μg mL^{-1} IgG1-PE (555749, Becton Dickinson, USA). The isotype control is a negative control to measure the concentration of EVs with non-specifically bound primary antibodies. To stop the reaction and prevent swarm detection,[21] the stained cell-depleted plasma was diluted 8-fold in PBS citrate.

Flow cytometry settings and analysis

All samples except the 200 nm gold nanoparticles were detected by an A50-Micro (Apogee Flow Systems, UK) during 60 seconds at a flow rate of 4.51 μL/min. The 200 nm gold nanoparticles were measured after the flow cytometer was upgraded to an A60-Micro. Whereas the A50-Micro is equipped with a 70 mW 405 nm laser, the A60-Micro is equipped with a 200 mW 405 nm laser and an improved obscuration bar. To compensate for the improved sensitivity, the 200 nm gold nanoparticles were measured at a laser power of 50 mW. The trigger threshold was set on FSC or SSC. Supplementary Table 3 shows the applied detector settings for all measurements. Data processing and representation were done with MATLAB R2011b (Mathworks, USA) and ORIGINPRO 8.5.0 (OriginLab Corporation, USA).

The symbols in Figure 2, *A* and *B* represent the mean diameter (Supplementary Table 1) and scattering intensity of each bead population. The mean scattering intensity was obtained by fitting the histogram of scattering intensities with a Gaussian function. The horizontal error bars represent the standard deviation of the size distribution (Supplementary Table 1). The vertical error bars represent the measurement error, defined as the mean coefficient of variation of the mean scattering intensities of 400 nm, 600 nm, 799 nm, and 994 nm polystyrene beads, which were measured 18 times during 45 days.

In Figure 4*C*, a fluorescence gate of 25 a.u. was used to select CD61+ EVs. Supplementary Figure 2, *A* and *B* show a scatter plot of PE-fluorescence versus FSC for the IgG1 control and the cell-depleted supernatant of a platelet concentrate, respectively.

Light scattering calculations

The power of light P scattered in the direction of a scatter detector (Figure 2, *A* and *B*) by a spherical particle with diameter d and RI n_p is given by:

$$P = F \iint_{\Omega_{FSC,SSC}} \frac{\eta(|S_2|^2 \cos\phi^2 + |S_1|^2 \sin\phi^2)}{k^2} sin\theta d\theta d\phi \qquad (1)$$

where Ω represents the solid angles of the FSC or SSC detector, F is a factor to scale the calculations to the data, η is the angle dependent transmission efficiency of the objective, S_1 and S_2 are the amplitude scattering matrix elements, θ the polar angle, ϕ the azimuthal angle, and $k = 2\pi n_m/\lambda$ the wavenumber for a medium with an RI of n_m at wavelength λ.[24,25] For water, n_m = 1.343 @405 nm and n_m = 1.337 @488 nm.[26] For PBS, n_m = 1.345 @405 nm and n_m = 1.339 @488 nm.[27] Estimates of Ω were either measured or obtained from datasheets and patents of the manufacturer.[28] To find the optimal values for Ω and F, a least square fit was applied on data from beads of known diameter and RI (Supplementary Table 1). S_1 and S_2 depend on d, n_p, n_m, k, and θ, and were calculated using the MATLAB scripts of Mätzler.[29] Since η decreases with increasing propagation angle α with respect to the optical axis of a microscope objective having aperture α_{max}, a sine function was chosen empirically as a weighting function for η[30]

$$\eta = \sin\left(\frac{\pi\alpha}{2\alpha_{max}} + \frac{1}{2}\pi\right) \qquad (2)$$

Flow cytometry scatter ratio (Flow-SR)

The flow cytometry scatter ratio (Flow-SR; Figure 2*C*) is the ratio between SSC and FSC. To obtain the size distribution of the bead mixture (Figure 3, *B* and *C*), a lookup table of Flow-SR versus d (Δd = 1 nm) of polystyrene was calculated (Figure 2*C*). The measured Flow-SR was related to d by linear interpolation. Because the lookup table has unique solutions for 0.53 ≤ Flow-SR ≤ 4.29 and d ≤ 560 nm, events with a Flow-SR < 0.53 or a Flow-SR > 4.29 were omitted. Beads > 560 nm were not present in the mixture.

To obtain the RI distribution of the bead mixture (Figure 3, *B* and *D*), a lookup table of FSC versus d (1 ≤ d ≤ 560 nm, Δd = 1 nm, 1.345 ≤ RI ≤ 2.000, ΔRI = 0.001) was calculated

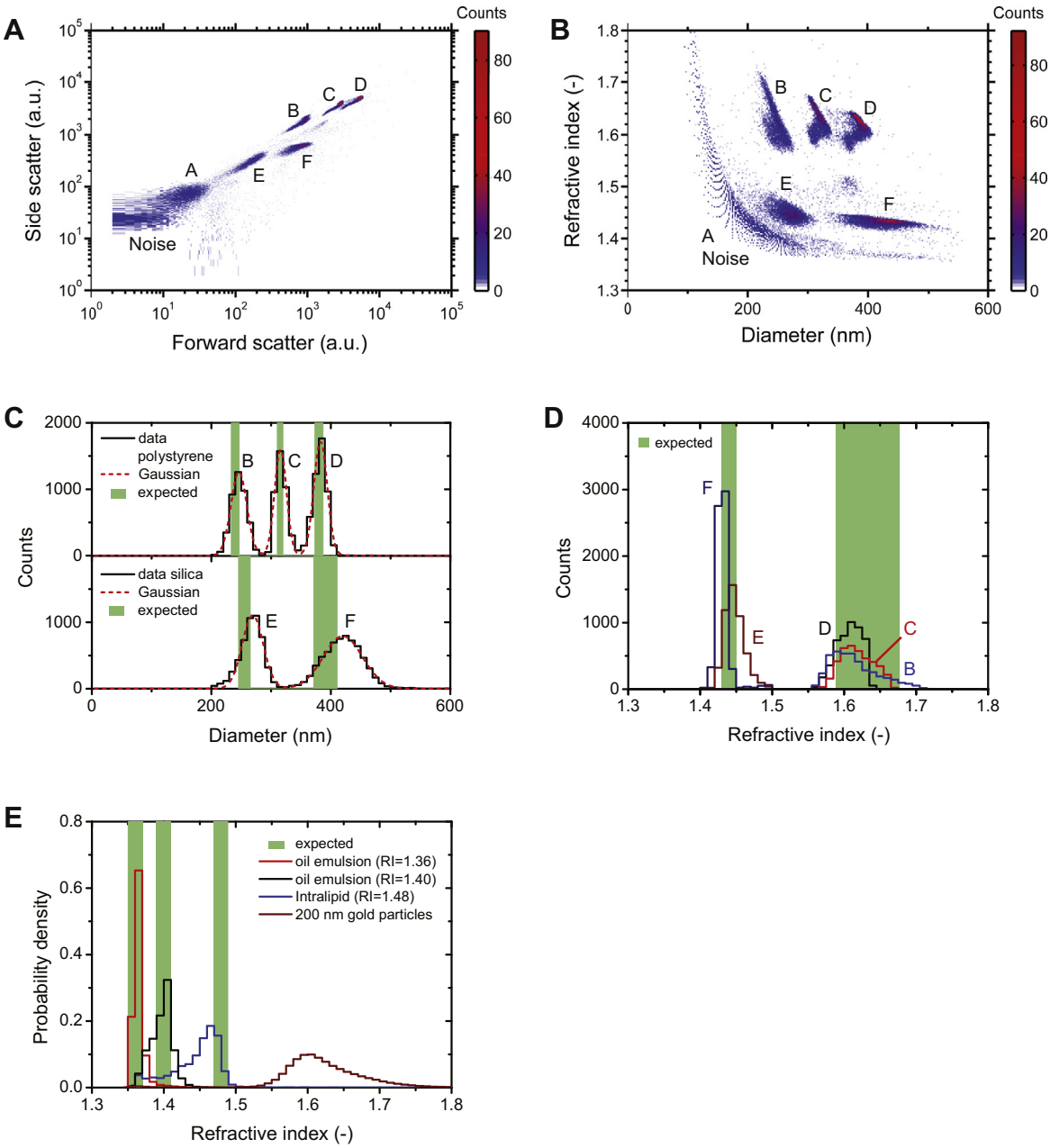

Figure 3. Validation of size and refractive index (RI) determination of nanoparticles by the flow cytometry scatter ratio (Flow-SR) using a bead mixture containing (**A**) 125 nm, (**B**) 240 nm, (**C**) 315 nm, and (**D**) 380 nm polystyrene beads and (**E**) 255 nm, and (**F**) 391 nm silica beads, oil emulsions, Intralipid, and gold nanoparticles. (**a**) Scatter plot of side scatter versus forward scatter of the bead mixture. Due to the arbitrary units (a.u.), the diameter and RI of the beads are unknown. (**b**) Scatter plot of RI versus diameter of the bead mixture. The diameter is obtained from Flow-SR (Figure 2*C*). The RI is derived from a lookup table of forward scatter versus diameter (Figure 2*A*). Bead populations B-F are clearly differentiated by size and RI. Bead population A and background noise result in a horizontal and vertical asymptote, caused by the detection thresholds and limited resolution of the flow cytometer. Panel (**a**) and (**b**) share the same scale bar. (**c**) Size distributions of the bead mixture (solid lines) fitted by Gaussian distributions (dotted lines). The bin width is 10 nm. The vertical bars indicate the reference size as mean ± standard deviation. (**d**,**e**) RI distributions (lines) of the bead mixture and oil emulsions, Intralipid, and 200 nm gold nanoparticles. The vertical bars indicate the range of reported RIs from literature.[31–34,36] The bin width is 0.01.

(Figure 2*A*). The measured diameter and FSC were related to the RI by linear interpolation. Events with an RI > 2 were omitted. In total, 10 % of the events were omitted.

To obtain the size distributions of EVs and LPs from the cell-depleted supernatant of a platelet concentrate (Figure 4, *B* and *C*), a lookup table of Flow-SR versus d of silica was used (Figure 2*C*), which has unique solutions for $0.33 \leq$ Flow-SR ≤ 4.29 and $d \leq 640$ nm. Events with a Flow-SR < 0.33 or a Flow-SR > 4.29 were omitted. For the cell-depleted supernatant of a platelet concentrate, the concentration of nanoparticles > 640 nm is

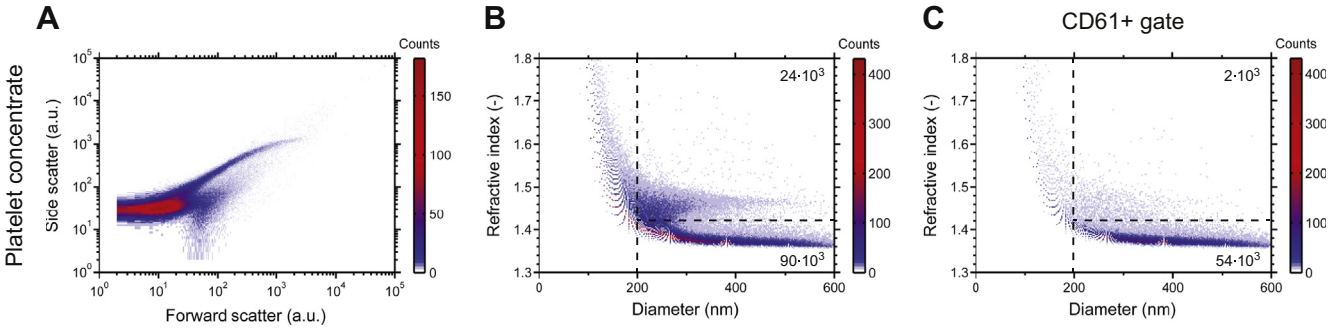

Figure 4. Application of the flow cytometry scatter ratio (Flow-SR) to extracellular vesicles (EVs) and lipoprotein particles (LPs) from the cell-depleted supernatant of a platelet concentrate. (**A**) Scatter plot of side versus forward scatter of EVs and LPs from the cell-depleted supernatant of a platelet concentrate. (**B**) Scatter plot of RI versus diameter of the same sample. For nanoparticles >200 nm (vertical dashed line), two populations are clearly differentiated by RI. The horizontal dashed line indicates an RI of 1.42. (**C**) Scatter plot of RI versus diameter of all CD61+ EVs from the same sample. From all CD61+ EVs >200 nm, 97% has an RI<1.42. Panel (**B**) and (**C**) share the same scale bar.

negligible.[9] The RI distribution was obtained similarly to the bead mixture. In total, 17.2 % of the ungated events and 4.8% of the CD61+ events were omitted.

Transmission electron microscopy

To confirm the presence of EVs and LPs in the cell-depleted supernatant of a platelet concentrate, 900 μL of cell-depleted plasma was thawed on ice and loaded on a Sepharose (CL-2B, GE Healthcare, Sweden) column of 10 mL.[11] Next, 10 μL of column fraction 9 was applied to a formfar-carbon coated 300 mesh grid (Electron Microscopy Sciences, USA) for 7 minutes, followed by staining with 1.75 % (w/v) uranyl acetate for 7 minutes. The sample was allowed to dry at room temperature for 2 hours and imaged with a transmission electron microscope (Technai-12, FEI, The Netherlands).

To obtain the reference values for the silica bead sizes in Supplementary Table 1, beads were diluted in 50 nm filtered (Nuclepore) purified and deionized water (MilliPore) to a concentration of ~10^8 mL^{-1}. To prevent aggregation of beads, 0.6 mM sodium dodecyl sulphate was added. Next, 7 μL of the solutions were added to formvar-carbon coated 300 mesh grids (Electron Microscopy Sciences, Hatfield, USA). After complete water evaporation, beads were imaged with a transmission electron microscope (CM-10, Philips, The Netherlands). From at least 1,000 beads of each population, the surface area per particle was determined with the Analyze Particles function of ImageJ (1.50i, National Institutes of Health, USA). Subsequently, the diameter was calculated from the surface area of each bead to create a size distribution. The size distributions were fitted by Gaussian functions to obtain the reference mean diameter and standard deviation.

Accuracy and precision

Accuracy is provided by the measurement error, defined as the measured mean value divided by the reference value (Supplementary Table 1) times 100%. Precision is provided by the coefficient of variation (CV) of the flow cytometry measurement, given by:

$$\mathrm{CV} = \sqrt{\left(\frac{\sigma_m}{\mu_m}\right)^2 - \left(\frac{\sigma_s}{\mu_s}\right)^2} \cdot 100\% \qquad (3)$$

where σ_m and σ_s are the measured and reference (Supplementary Table 1) standard deviations, respectively, and μ_m and μ_s are the measured and reference (Supplementary Table 1) mean values, respectively.

Results

From arbitrary units to size and RI

To relate FSC and SSC to the diameter and RI of single nanoparticles, we measured the FSC and SSC for polystyrene and silica beads with known diameter and RI (Supplementary Table 1). We described the data by Mie theory,[25] incorporating the diameter and RI of the nanoparticle, the RI of the medium, and the optical configuration of the flow cytometer[9,21] (see Supporting information). Figure 2, *A* and *B* show that the theory describes the data well ($R^2 \geq 0.98$ for polystyrene and $R^2 \geq 0.93$ for silica) and that the measured FSC or SSC cannot be uniquely related to both the diameter and RI of the nanoparticle.

To obtain the diameter *independent* of the RI of a nanoparticle, we took the ratio between SSC and FSC, which we named the flow cytometry scatter ratio (Flow-SR). Figure 2*C* shows that the Flow-SR versus diameter relationship is independent of the RI for nanoparticles with a diameter ≤1.2-fold the illumination wavelength of 405 nm. For example, because a nanoparticle with FSC 90 and SSC 225 has a Flow-SR of 2.5, its diameter is 200 nm regardless of the RI (Figure 2*C*, arrows). After the diameter is obtained by Flow-SR, a lookup table of scatter versus diameter can be used to derive the RI.[24] For example, a nanoparticle of 200 nm with FSC 90 has an RI of 1.50 (Figure 2*A*, arrows). Thus, Flow-SR and Mie theory provide a tool to determine both the diameter and RI of spherical nanoparticles.

Validation of size and RI determination

To validate the capability of Flow-SR to determine the diameter and RI of single nanoparticles, we have measured FSC and SSC of a mixture of polystyrene and silica beads (Supplementary Table 2). The beads in the mixture differ from the beads used to calibrate the flow cytometer. Figure 3**a** shows the SSC-FSC scatter plot of the bead mixture. The 6 bead populations are clearly discernible, but the diameter and RI of the beads cannot be obtained from the plot. By applying Flow-SR, the diameter and RI of the beads were obtained, as shown in Figure 3**b**. Except for the 125 nm polystyrene beads, for which the flow cytometer lacked the required resolution to apply Flow-SR, each bead population is clearly discernible and correctly identified by diameter and RI.

To determine the sizing accuracy and precision, Figure 3**c** shows the size distribution of the polystyrene and silica beads. For all beads, the diameter was determined with ≤7% accuracy and ≤6% precision. For comparison, we previously obtained that nanoparticle tracking analysis has an accuracy ≤7% and a precision ≤17%, whereas tunable resistive pulse sensing has an accuracy ≤5% and a precision ≤7% in determining the diameter.[9]

Figure 3**d** shows the RI distribution of the bead mixture. Lack of reference materials with a traceable RI precludes the determination of accuracy and precision. However, the measured RI of the beads are within the range of previous estimates, which is 1.59-1.68 for polystyrene beads and 1.43-1.45 for silica beads.[31–34] The coefficient of variation of the RI distributions increases with decreasing size and ranges from 0.5% to 1.7%.

To further validate flow-SR, Figure 3**e** shows the measured RI distributions of emulsions containing oil droplets of RI 1.36 and 1.40 (#1475, Apogee Flow Systems, UK), Intralipid (Fresenius-Kabi, Germany), and 200 nm gold nanoparticles (742066, Sigma-Aldrich, Germany). The oil emulsions and Intralipid are polydisperse and contain particles with an RI resembling EVs[24,35] and lipoproteins,[36] respectively. The measured RI of these polydisperse samples matches the expectation values. Due to the presence of free electrons, gold nanoparticles have strong absorption (k=1.84-2.03)[37,38] and surface plasmons that increase the scattering efficiency. However, Figure 3**e** provides the RI of a dielectric sphere without absorption having the same scattering efficiency as 200 nm gold nanoparticles. Based on the measured complex RI of gold,[38] we expect 200 nm gold nanoparticles to scatter as efficiently as 200 nm non-absorbing dielectric spheres with an RI of 1.92. We attribute the underestimation of the RI to the uncertainty in the expected RI for gold nanoparticles,[39] a 26% overestimation of the determined mean diameter, and the presence of surfactants affecting the scattering properties of gold.

Label-free differentiation between EVs and LPs

Besides EVs, blood plasma contains an abundance of similar-sized LPs.[10,11] Because EVs and LPs differ in composition, and because the RI depends on the composition of a nanoparticle,[25] we hypothesize that EVs and LPs can be differentiated by RI using Flow-SR. To confirm our hypothesis, we have measured EVs and LPs from the cell-depleted supernatant of a platelet concentrate. Figure 4*A* shows the resulting SSC-FSC scatter plot. Because the data are expressed in arbitrary units, it remains unclear which data points correspond to the EVs of interest. Moreover, the scatter plot cannot be related to TEM data of the same sample (Figure 1*A*).

Figure 4*B* shows the RI-diameter scatter plot of the same sample after application of Flow-SR. Now, two populations are discernible based on their RI. Because the mode RI of platelet-derived EVs is expected to be 1.39[35] and the RI of LPs is >1.45,[36] we attribute events with an RI <1.42 (79%) to EVs and events with an RI >1.42 (21%) to LPs. The asymptotes are caused by the detection thresholds, with the vertical asymptote resulting in the apparent presence of nanoparticles with an RI>1.6. To avoid artifacts, we will focus on nanoparticles >200 nm for further analysis.

To confirm that events with an RI <1.42 are EVs and not LPs, we labeled EV with a fluorescent marker against CD61.[40–42] CD61 is a subunit of the platelet fibrinogen receptor and therefore expected to be present on platelet-derived EVs. Figure 4*C* shows that 97% of the CD61+ events indeed have an RI <1.42. Thereby, we demonstrate label-free differentiation between EVs and LPs.

Discussion

Here we present a new method, named Flow-SR, to relate the ambiguous light scattering signals of a flow cytometer to the absolute size and RI of single nanoparticles. Within the dynamic range of the scatter detectors, Flow-SR has higher accuracy (<7%) and precision (<6%) and is >100-fold faster than nanoparticle tracking analysis and tunable resistive pulse sensing, two commonly used techniques dedicated to sizing nanoparticles in solution.[9,18,24] Moreover, the introduction of the RI as a new label-free parameter for nanoparticles has three important consequences for EV research.

First, Flow-SR enables label-free differentiation between EVs (RI<1.42) and LPs (RI>1.42). The finding that platelet EVs[43] and LPs are spherical legitimates the application of Flow-SR. Hitherto, label-free differentiation between EVs and LPs was only possible with cryo electron microscopy,[22,43] an accurate but low throughput technique. However, even when flow cytometry in combination with membrane dye staining is used, both EVs and LPs may be stained due to similarities in membrane composition. RI-based differentiation, on the other hand, is expected to be more specific. Volume-wise, EVs primarily consist of water surrounded by a phospholipid bilayer.[22,24,42] Consequently, the effective RI of EVs is closer to water than the RI of other nanoparticles in blood, such as LPs, high molecular weight proteins, and protein aggregates. RI-based identification has therefore perspective to become a generic EV marker with high specificity. Because fluorescent antibodies may bind non-specifically to LPs, a specific generic EV marker will also improve the specificity of flow cytometry assays involving immunostaining. Using Flow-SR, we found a median RI of 1.37 for CD61+ EVs >200 nm. The measured RI of plasma EVs is similar to the RI of urinary EVs[24] and lies within the values expected from the concentric morphology and chemical composition of the EVs. Because an earlier study lacked the resolution to

differentiate between EV and LPs,[35] we claim to have measured the first RI distribution of EVs from blood plasma.

Second, access to the RI and diameter of EVs is of great value to data comparison and standardization. Especially because (1) the concentration of EVs increases with decreasing size,[9] and (2) flow cytometers differ in sensitivity, the measured EV concentration strongly depends on the dynamic size range of the flow cytometer. For example, a decrease in the minimum detectable EV size from 80 nm to 60 nm would result in a 2.4-fold increase in the obtained concentration.[9] Knowledge of the detected EV diameter is therefore essential to comparing the EV concentration between flow cytometers. A study involving multiple flow cytometers with nanoparticle sensitivity on both the FSC and SSC detector is required to show whether diameter estimation by Flow-SR improves data comparison. Knowledge of the RI may improve standardization initiatives that include flow cytometers that lack the sensitivity for Flow-SR. For example, the measured median RI of 1.37 of plasma EVs can be used to relate light scattering of one channel to the diameter of EVs by Mie theory.

Third, Flow-SR improves data interpretation. For example, the size and RI representation of Figure 4, *B* and *C* reveal that the light scattering signals of EVs just exceed the detection threshold of the flow cytometer. Consequently, flow cytometry and TEM detect entirely different sizes of EVs: whereas flow cytometry detects the relatively low concentration of EVs >200 nm, TEM primarily images smaller EVs. In addition, for the size range 200-400 nm, we show that the concentrations of EVs and LPs in platelet concentrates have the same other of magnitude. This is remarkable, because in blood plasma the EV concentration in the size range ~60-200 nm is at least 2 orders of magnitude lower than the LP concentration.[10]

Compared to previous approaches to determine the size and RI of particles by flow cytometry,[30,44] Flow-SR is easier to implement. Because Flow-SR is applicable to all instruments with nanoparticle sensitivity on the FSC and SSC detector (Supplementary Figure 1*A*), Flow-SR does not require hardware modifications, whereas for example scanning flow cytometry requires a specialized setup to enable the detection of angle dependent light scattering.[44] Furthermore, Flow-SR is solely based on taking the ratio between SSC and FSC and applying Mie theory, for which documentation and scripts are widely available, whereas a previous approach required empirical corrections.[30] In previous approaches, the smallest detectable particles were 570 nm and 900 polystyrene beads.[30,44] For our flow cytometer, Flow-SR is applicable to spherical nanoparticles between 200-500 nm with an RI>~1.36. Application to smaller nanoparticles or nanoparticles with an RI closer to water is theoretically possible but requires a more sensitive system and additional research. Detection of larger particles can be accomplished by using a longer wavelength, because the angular light scattering distribution depends on the ratio between the particle diameter and the wavelength (Supplementary Figure 1*B*). For gold nanoparticles, we obtained a 26% overestimation of the mean diameter and therefore an underestimation of the RI. However, only the gold nanoparticles were characterized by the Apogee A60-Micro, which had a misaligned laser during this particular experiment. The application of Flow-SR to metal nanoparticles therefore requires further investigation.

Because Flow-SR is relatively easy to implement, widely applicable, accurate and fast, we expect immediate applications in nanotechnology. Here, we demonstrated RI-based differentiation between EVs and LPs, polydisperse oil emulsions, Intralipid, and 200 nm gold nanoparticles. In environmental science, pollen (RI ≈ 1.53)[45] could be distinguished from harmful cement dust (RI ≈ 1.70),[46] fly ash (RI = 1.55−1.60),[47] metal nanoparticles, or nanoplastics without labeling. In food production, label-free monitoring of the concentration of EVs and milk fat globules in cow milk or infant formula may improve quality control. In nanomedicine, drug-containing liposomes may be identified by RI and separated from empty liposomes using flow cytometers with sorting capability. Compared to immunostaining, RI-based differentiation of nanoparticles is less specific but faster, cheaper, and harmless for biologically active particles. Moreover, within the dynamic range of the scatter detectors, data on EVs can be interpreted and compared between flow cytometers, other analytical methods, and clinical laboratories. In metrology, Flow-SR may be used to certify reference nanoparticles.[23] Thus, Flow-SR has the potential to contribute to all disciplines where absolute sizing and identification of single nanoparticles is essential.

Appendix A. Suppplementary data

Supplementary data to this article can be found online at https://doi.org/10.1016/j.nano.2017.12.012.

References

1. van der Pol E, Boing AN, Harrison P, Sturk A, Nieuwland R. Classification, Functions, and Clinical Relevance of Extracellular Vesicles. *Pharmacol Rev* 2012;**64**(3):676-705.
2. Hoshino A, Costa-Silva B, Shen TL, Rodrigues G, Hashimoto A, Tesic Mark M, et al. Tumour exosome integrins determine organotropic metastasis. *Nature* 2015;**527**(7578):329-35.
3. Melo SA, Luecke LB, Kahlert C, Fernandez AF, Gammon ST, Kaye J, et al. Glypican-1 identifies cancer exosomes and detects early pancreatic cancer. *Nature* 2015;**523**(7559):177-82.
4. Krafft C, Wilhelm K, Eremin A, Nestel S, von Bubnoff N, Schultze-Seemann W, et al. A specific spectral signature of serum and plasma-derived extracellular vesicles for cancer screening. *Nanomedicine* 2017;**13**(3):835-41.
5. Owens III AP, Mackman N. Microparticles in hemostasis and thrombosis. *Circ Res* 2011;**108**(10):1284-97.
6. Agrawal AK, Aqil F, Jeyabalan J, Spencer WA, Beck J, Gachuki BW, et al. Milk-derived exosomes for oral delivery of paclitaxel. *Nanomedicine* 2017;**13**(5):1627-36.
7. Bell BM, Kirk ID, Hiltbrunner S, Gabrielsson S, Bultema JJ. Designer exosomes as next-generation cancer immunotherapy. *Nanomedicine* 2016;**12**(1):163-9.
8. Roma-Rodrigues C, Pereira F, Alves de Matos AP, Fernandes M, Baptista PV, Fernandes AR. Smuggling gold nanoparticles across cell types - A new role for exosomes in gene silencing. *Nanomedicine* 2017;**13**(4):1389-98.
9. van der Pol E, Coumans FA, Grootemaat AE, Gardiner C, Sargent IL, Harrison P, et al. Particle size distribution of exosomes and microvesicles

determined by transmission electron microscopy, flow cytometry, nanoparticle tracking analysis, and resistive pulse sensing. *J Thromb Haemost* 2014;**12**(7):1182-92.
10. Dragovic RA, Gardiner C, Brooks AS, Tannetta DS, Ferguson DJ, Hole P, et al. Sizing and phenotyping of cellular vesicles using Nanoparticle Tracking Analysis. *Nanomedicine* 2011;**7**(6):780-8.
11. Boing AN, van der Pol E, Grootemaat AE, Coumans FA, Sturk A, Nieuwland R. Single-step isolation of extracellular vesicles by size-exclusion chromatography. *J Extracell Vesicles* 2014;**3**:23430.
12. Yuana Y, Levels J, Grootemaat AE, Sturk A, Nieuwland R. Co-isolation of extracellular vesicles and high-density lipoproteins using density gradient ultracentrifugation. *J Extracell Vesicles* 2014;**3**:23262.
13. Nordin JZ, Lee Y, Vader P, Mager I, Johansson HJ, Heusermann W, et al. Ultrafiltration with size-exclusion liquid chromatography for high yield isolation of extracellular vesicles preserving intact biophysical and functional properties. *Nanomedicine* 2015;**11**(4):879-83.
14. Vickers KC, Palmisano BT, Shoucri BM, Shamburek RD, Remaley AT. MicroRNAs are transported in plasma and delivered to recipient cells by high-density lipoproteins. *Nat Cell Biol* 2011;**13**(4):423-33.
15. Wagner J, Riwanto M, Besler C, Knau A, Fichtlscherer S, Roxe T, et al. Characterization of levels and cellular transfer of circulating lipoprotein-bound microRNAs. *Arterioscler Thromb Vasc Biol* 2013;**33**(6):1392-400.
16. van der Pol E, Boing AN, Gool EL, Nieuwland R. Recent developments in the nomenclature, presence, isolation, detection and clinical impact of extracellular vesicles. *J Thromb Haemost* 2016;**14**(1):48-56.
17. Pasalic L, Williams R, Siupa A, Campbell H, Henderson MJ, Chen VM. Enumeration of extracellular vesicles by a new improved flow cytometric method is comparable to fluorescence mode nanoparticle tracking analysis. *Nanomedicine* 2016;**12**(4):977-86.
18. Gardiner C, Di Vizio D, Sahoo S, Théry C, Witwer KW, Wauben M, et al. Techniques used for the isolation and characterization of extracellular vesicles: results of a worldwide survey. *J Extracell Vesicles* 2016;**5**:32945.
19. Nolte-'t Hoen EN, van der Vlist EJ, Aalberts M, Mertens HC, Bosch BJ, Bartelink W, et al. Quantitative and qualitative flow cytometric analysis of nanosized cell-derived membrane vesicles. *Nanomedicine* 2012;**8**(5):712-20.
20. Gasecka A, Boing AN, Filipiak KJ, Nieuwland R. Platelet extracellular vesicles as biomarkers for arterial thrombosis. *Platelets* 2016:1-7.
21. van der Pol E, van Gemert MJ, Sturk A, Nieuwland R, van Leeuwen TG. Single vs. swarm detection of microparticles and exosomes by flow cytometry. *J Thromb Haemost* 2012;**10**(5):919-30.
22. Arraud N, Linares R, Tan S, Gounou C, Pasquet JM, Mornet S, et al. Extracellular vesicles from blood plasma: determination of their morphology, size, phenotype and concentration. *J Thromb Haemost* 2014;**12**(5):614-27.
23. Nicolet A, Meli F, van der Pol E, Yuana Y, Gollwitzer C, Krumrey M, et al. Inter-laboratory comparison on the size and stability of monodisperse and bimodal synthetic reference particles for standardization of extracellular vesicle measurements. *Meas Sci Technol* 2016;**27**(3).
24. van der Pol E, Coumans FA, Sturk A, Nieuwland R, van Leeuwen TG. Refractive index determination of nanoparticles in suspension using nanoparticle tracking analysis. *Nano Lett* 2014;**14**(11):6195-201.
25. Bohren CF, Huffman DR. *Absorption and scattering of light by small particles*. New York, USA: Wiley; 1983 [XIV, 530 S. p.].
26. Daimon M, Masumura A. Measurement of the refractive index of distilled water from the near-infrared region to the ultraviolet region. *Appl Optics* 2007;**46**(18):3811-20.
27. Xu SH, Liu H, Sun ZW. Optical factors determined by the T-matrix method in turbidity measurement of absolute coagulation rate constants. *J Colloid Interface Sci* 2006;**304**(1):107-14.
28. Kenyon O, inventor; OJK Consulting LTD, assignee. Method and system for calibrating a flow cytometer. United Kingdom2015.
29. Mätzler C. *MATLAB functions for Mie scattering and absorption*. Bern, Zwitzerland: Institut für Angewandte Physik, Univeristy of Bern; 2002 [Contract No.: 2002-08].
30. Green RE, Sosik HM, Olson RJ, DuRand MD. Flow cytometric determination of size and complex refractive index for marine particles: comparison with independent and bulk estimates. *Appl Optics* 2003;**42**(3):526-41.
31. Knoner G, Parkin S, Nieminen TA, Heckenberg NR, Rubinsztein-Dunlop H. Measurement of the index of refraction of single microparticles. *Phys Rev Lett* 2006;**97**(15):157402.
32. Miles REH, Rudic S, Orr-Ewing AJ, Reid JP. Measurements of the wavelength dependent extinction of aerosols by cavity ring down spectroscopy. *Phys Chem Chem Phys* 2010;**12**(15):3914-20.
33. Kasarova SN, Sultanova NG, Ivanov CD, Nikolov ID. Analysis of the dispersion of optical plastic materials. *Opt Mater* 2007;**29**(11):1481-90.
34. Hart SJ, Terray AV. Refractive-index-driven separation of colloidal polymer particles using optical chromatography. *Appl Phys Lett* 2003;**83**(25):5316-8.
35. Gardiner C, Shaw M, Hole P, Smith J, Tannetta D, Redman CW, et al. Measurement of refractive index by nanoparticle tracking analysis reveals heterogeneity in extracellular vesicles. *J Extracell Vesicles* 2014;**3**:25361.
36. Mills GL, Lane PA, Weech PK. In: Burdon RH, Knippenberg PH, editors. *A guidebook to lipoprotein techniques*. Amsterdam, The Netherlands: Elsevier; 2000.
37. Werner WSM, Glantschnig K, Ambrosch-Draxl C. Optical Constants and Inelastic Electron-Scattering Data for 17 Elemental Metals. *J Phys Chem Ref Data Monogr* 2009;**38**(4):1013-92.
38. Rakic AD, Djurisic AB, Elazar JM, Majewski ML. Optical properties of metallic films for vertical-cavity optoelectronic devices. *Appl Optics* 1998;**37**(22):5271-83.
39. Ungureanu C, Amelink A, Rayavarapu RG, Sterenborg HJCM, Manohar S, van Leeuwen TG. Differential Pathlength Spectroscopy for the Quantitation of Optical Properties of Gold Nanoparticles. *ACS Nano* 2010;**4**(7):4081-9.
40. Shah MD, Bergeron AL, Dong JF, Lopez JA. Flow cytometric measurement of microparticles: Pitfalls and protocol modifications. *Platelets* 2008;**19**(5):365-72.
41. Lacroix R, Robert S, Poncelet P, Kasthuri RS, Key NS, Dignat-George F, et al. Standardization of platelet-derived microparticle enumeration by flow cytometry with calibrated beads: results of the International Society on Thrombosis and Haemostasis SSC Collaborative workshop. *J Thromb Haemost* 2010;**8**(11):2571-4.
42. Arraud N, Gounou C, Turpin D, Brisson AR. Fluorescence Triggering: A General Strategy for Enumerating and Phenotyping Extracellular Vesicles by Flow Cytometry. *Cytometry A* 2016;**89a**(2):184-95.
43. Brisson AR, Tan S, Linares R, Gounou C, Arraud N. Extracellular vesicles from activated platelets: a semiquantitative cryo-electron microscopy and immuno-gold labeling study. *Platelets* 2017:1-9.
44. Maltsev VP. Scanning flow cytometry for individual particle analysis. *Rev Sci Instrum* 2000;**71**(1):243-55.
45. Charriere F, Marian A, Montfort F, Kuehn J, Colomb T, Cuche E, et al. Cell refractive index tomography by digital holographic microscopy. *Opt Lett* 2006;**31**(2):178-80.
46. Ferraris CF, Guthrie W, Avilés AI, Peltz M, Haupt R, MacDonald BS. Certification of SRM 114q: Part II (Particle size distribution). *NIST Special Publication*, 260. ; 2006. p. 166.
47. Jewell RB, Rathbone RF. Optical properties of coal combustion byproducts for particle-size analysis by laser diffraction. *Combust Gasification Prod* 2009;**1**:1-6.